COO-4246-7

MICROSTRUCTURAL EFFECTS IN ABRASIVE WEAR

Quarterly Progress Report
for the period 15 September 1978 - 15 December 1978

Nicholas F. Fiore, Thomas H. Kosel, Stephen Udvardy and
William Konkel

Department of Metallurgical Engineering and Materials Science
Notre Dame, IN 46556

NOTICE

This report was prepared as an account of work sponsored by the United States Government. Neither the United States nor the United States Department of Energy, nor any of their employees, nor any of their contractors, subcontractors, or their employees, makes any warranty, express or implied, or assumes any legal liability or responsibility for the accuracy, completeness, or usefulness of any information, apparatus, product or process disclosed or represents that its use would not infringe privately owned rights.

15 January 1979

Prepared for

U. S. Department of Energy

Under Contract No. EF-77-S-02-4246

DISCLAIMER

ABSTRACT

The purpose of this research project is to establish reliable low-stress and gouging wear rate information for a series of alloy white irons and a series of Co-base PM alloys and to correlate the wear resistance with the microstructural features and mechanical properties of these materials.

Past work has involved the characterization of wear rates and microstructures of the alloys. In this quarter, SEM characterization of the wear scars has been undertaken with the intent of understanding the different responses of the alloys to the different testing conditions. Both RWAT and GAWT wear scars in Ni-Hard 4 were examined. The results of these observations were clarified after SEM/EDXS analysis of the RWAT and GAWT wear scars in the Stellite 6 alloy, in which the carbide positions in the worn surface were found using EDXS x-ray maps.

The carbides protrude from the worn surfaces in all RWAT wear scars examined to date, including those of the Ni-Hard 4 alloys abraded with SiO_2 and the Stellite 6 alloy abraded with SiO_2 and Al_2O_3. The harder Al_2O_3 abrasive particles leave long continuous grooves in the surface of the Stellite 6 alloy, and they partially penetrate the Cr_7C_3 carbides. In the GAWT test, some of the alloy carbides are cut off flush with the worn matrix surface, while some undergo gross fracture and are removed in large fragments.

Although quantitative ranking of the wear resistance of alloys is not yet possible by SEM analysis, useful qualitative generalizations may be made.

CONTENTS

ABSTRACT i

1. OBJECTIVE AND SCOPE 1

2. TASKS AND PROGRESS 1

2.1 Task I - Preparation of Test Matrix 1

2.2 Task II - Preparation of Materials 1

2.3 Task III - Wear Testing 2

2.3.1 Wear Testing of Ni-Hard 4 2

2.3.2 Wear Testing of the Co-base PM Alloys 4

2.3.3 Degradation of the RWAT Abrasives 5

2.4 Task IV - Wear Scar and Microstructure Characterization 8

2.4.1 Optical and Quantitative Metallography of the Co-base PM Alloys 8

2.4.2 SEM Observations of Ni-Hard 4 Wear Scars 9

2.4.2.1 Ni-Hard 4 SiO_2 RWAT Wear Scars 9

2.4.2.2 Ni-Hard 4 GAWT Wear Scars 15

2.4.3 SEM/EDXS Observations of Co-base PM Alloy Wear Scars 20

2.4.3.1 Co-base Alloy RWAT Wear Scars 20

2.4.3.2 Co-base Alloy GAWT Wear Scars 25

2.5 Task V - Analysis of Data 29

2.5.1 Ni-Hard 4 SEM Observations 29

2.5.2 Co-base PM Alloy SEM Observations 30

3. SUMMARY 31

4. PERSONNEL 32

LIST OF FIGURES 33

1. OBJECTIVE AND SCOPE

This work is directed at establishing quantitative relations between microstructure and wear resistance of low-to-high Cr white irons (ASTM Series 532) and Co-base powder metallurgy (PM) alloys commonly used in coal conversion processes. The research involves study of gouging wear resistance, such as is necessary in mining operations, and low-stress abrasion resistance, such as required in coal and coal-product handling and transfer operations. The project has both applied and basic aspects. On the applied side, the establishment of the optimum microstructures for wear resistance will allow (and is already beginning to allow) design engineers to make more effective decisions regarding candidate alloys for coal-related processes. From the basic viewpoint, the establishment of a better understanding of the physical and mechanical metallurgy of wear may lead in the longer run to the development of more economical and effective wear-resistant alloys.

This project has been in existence for about 21 months. Most of the testing and analysis done during the first 18 months of the project was on the white irons, and since that time the work has focussed on the cobalt-based PM alloys. The wear test results on these alloys were summarized in the last quarterly report, COO-4246-6.

The present work concerns itself mainly with attempts to characterize and understand the wear scars using scanning electron microscopy (SEM) in combination with energy-dispersive x-ray spectroscopy (EDXS).

2. TASKS AND PROGRESS

2.1 Task I - Preparation of Test Matrix

Task completed 6 June 1977.

2.2 Task II - Preparation of Materials

Task completed 15 March 1978.

The white iron and Co-base alloy materials have been obtained. The compositions, heat treatments and microstructures of the white irons have been discussed in the quarterly report COO-4246-4, and a similar discussion for the Co-base alloys has been given in quarterly report COO-4246-5.

2.3 Task III - Wear Testing

The results of wear testing of the Ni-Hard 4 alloy and of the Co-base PM alloys were completed and described in earlier reports, and are repeated here for discussion with respect to current SEM observations.

The gouging wear test (GAWT) is performed with a bonded Al_2O_3 abrasive wheel, and the low stress abrasion test (RWAT) with a rubber wheel abrasive testing apparatus. Either SiO_2 or Al_2O_3 abrasive is used with the RWAT. Both tests have been previously described in quarterly report #2 (COO-4246-2).

2.3.1 Wear Testing of Ni-Hard 4.

The Ni-Hard 4 alloy was heat treated to obtain four different microstructures containing 5, 20, 40 and 85 percent retained austenite. These microstructures were discussed in quarterly report #4 and are included in Figure 1 of this report for comparison with SEM micrographs.

The results of wear testing of this alloy were presented in quarterly reports #3 and #4 and these results are summarized here in Figure 2, which includes both Al_2O_3 and SiO_2 RWAT results as well as GAWT results and the AMAX Pin Test (A.P.T.) results with two abrasives. The amount of retained austenite decreases to the right in this plot. The maxima and minima of the wear curves occur at 40 percent retained austenite in each case. Since testing with the GAWT and the SiO_2 RWAT tests produced consistently opposite trends of wear rate versus various mechanical properties in this series of microstructures (quarterly #3), it was decided to conduct RWAT tests with Al_2O_3 abrasive. This resulted

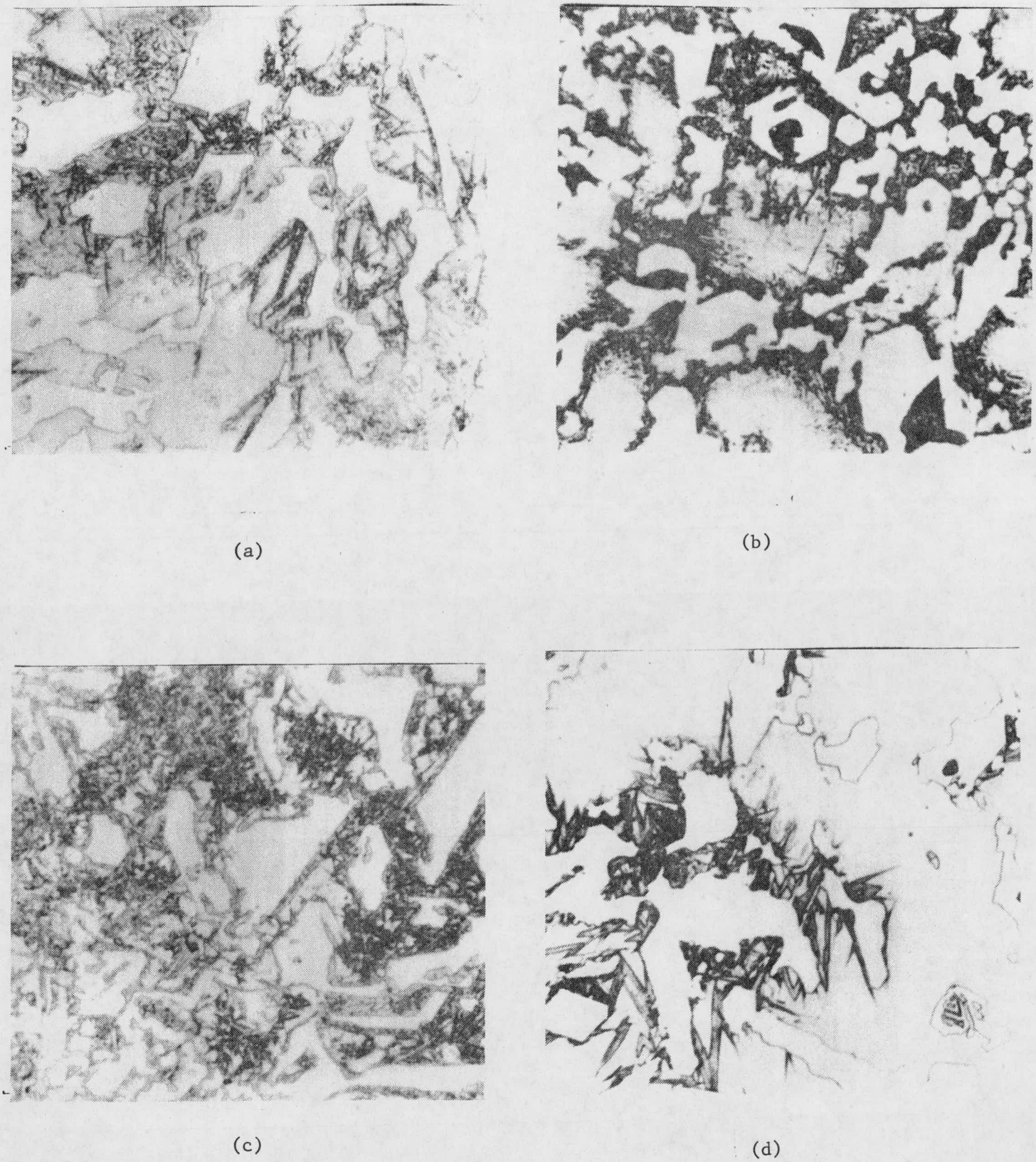

(a) (b)

(c) (d)

Figure 1. Microstructures resulting from the four different heat treatments of the Ni-Hard 4 cast iron. M_7C_3 carbides (white) in matrices of various percentages of retained austenite with austenite decomposition products. (a) 5% γ; (b) 20% γ; (c) 40% γ; (d) 85% γ. All are at 900X.

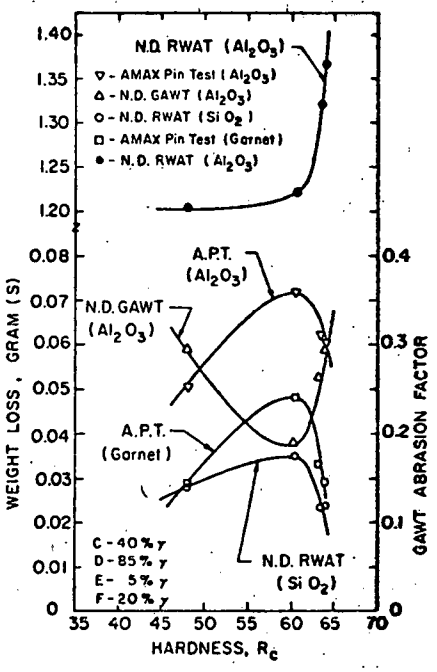

Figure 2. RWAT, APT, and GAWT test results on Ni-Hard 4 samples. The percent retained austenite decreases toward the right.

in wear rates which resemble the GAWT results in their trend more nearly than the SiO_2 RWAT results, which suggested that the hardness of the abrasive was probably more important in producing the observed trend reversal than was the change from low stress to gouging wear conditions.

2.3.2 Wear Testing of the Co-base PM Alloys

The compositions and microstructures of the six Co-base PM alloys used in this work have been discussed previously in quarterlies #5 and #6. These commercially relevant alloys comprise a system in which increasing carbide volume fractions are found in matrices of increasing solid solution strengthener contents.

The GAWT and SiO_2 RWAT wear test data for these alloys were shown in the last quarterly (#6) to exhibit a minimum when the wear rate is plotted either against carbide volume fraction or against normalized alloy content, whereas the Al_2O_3 RWAT data show a monotomic decrease in wear rate with these two parameters. The plots of wear rates versus carbide volume fraction for the

different tests are included here in Figures 3 and 4.

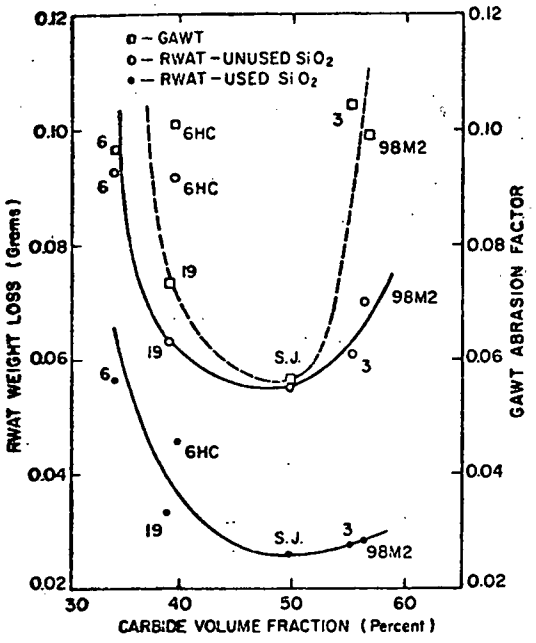

Fig. 3. GAWT abrasion factor and RWAT weight loss (unused and used SiO_2) versus carbide volume fraction.

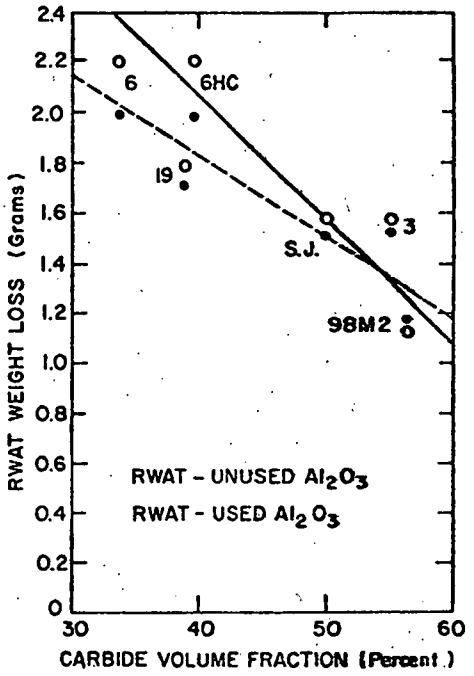

Fig. 4. RWAT weight loss (unused and used Al_2O_3) versus carbide volume fraction.

In this quarter, SEM/EDXS studies of the wear scars have been initiated in an effort to understand the mechanisms which give rise to the wear behavior shown in Figures 3 and 4. The preliminary results of these studies are described in Section 2.4.3 of this report.

2.3.3 Degradation of RWAT Abrasives

As we discussed previously in quarterlies #3 and #6, both SiO_2 and Al_2O_3 abrasives undergo significant size reductions during the RWAT test. Consequently a systematic investigation into the effect of this degradation on the wear rates of the Co-base PM alloys was undertaken. The alloys were each tested against new SiO_2 and Al_2O_3 and then against SiO_2 and Al_2O_3 which had been used in one prior RWAT test. The sieve analyses of the new and used

abrasives are displayed in Figures 5a,b.

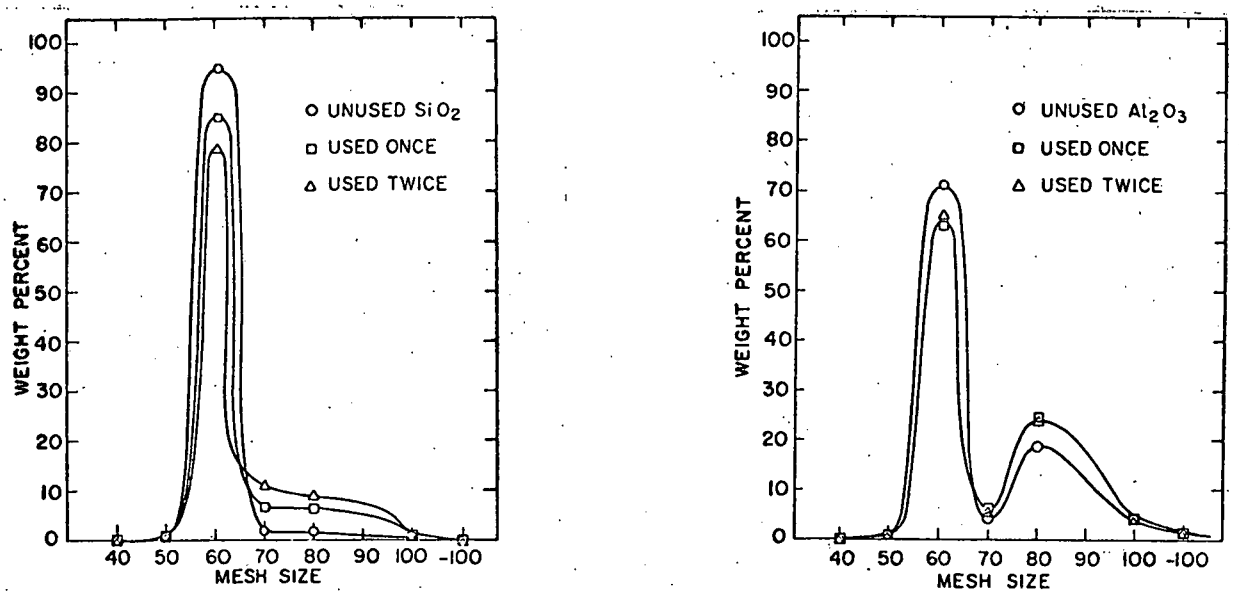

(a) (b)

Figure 5. Sieve analyses of new and used RWAT abrasives. (a) SiO_2 and (b) Al_2O_3.

Since the RWAT test was designed to simulate abrasion under conditions which do not lead to degradation of the abrasive particles, it was felt that it was necessary to further investigate the degradation of the abrasive by the RWAT. Therefore, part of the effort this quarter was spent in an attempt to determine the nature of the degradation of the abrasive by the application of SEM. Low-magnification SEM micrographs of the new and used SiO_2 and Al_2O_3 abrasives are shown in Figure 6. The difficulties in determining the underlying cause of the reduction in the abrasiveness of these particles by SEM observations is evident. Individual particles vary so much that small overall changes in the average particle size and shape may not be distinguished. The problem is really a statistical one, and although relatively small changes in size distribution can be examined by sieve analysis of very large numbers of particles, no comparably

(a)

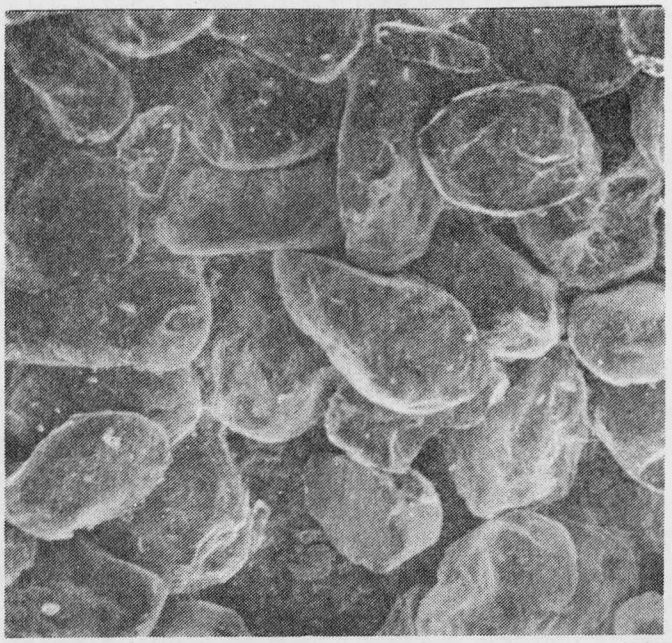

(b)

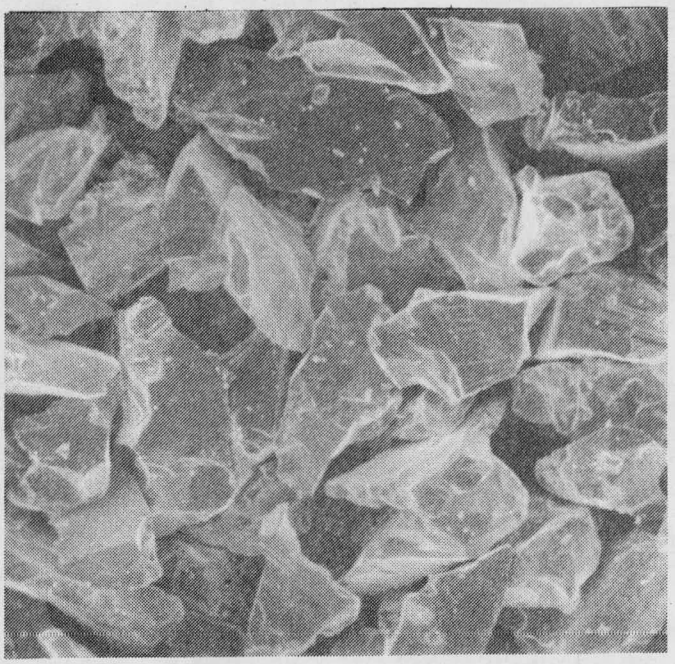

(c)

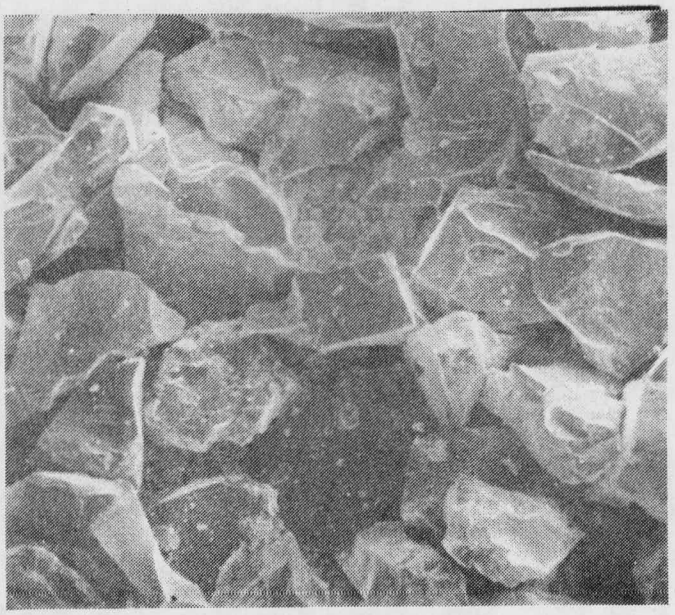

(d)

Figure 6. 60X SEM micrographs of new and used RWAT abrasives. (a) New SiO_2, (b) SiO_2, used twice, (c) new Al_2O_3, and (d) Al_2O_3, used twice.

simple method exists for the determination of small differences in average shape.

Higher magnification observations of the SiO_2 abrasives revealed some areas in which local melting of the abrasive may have occurred, since it appeared that the material had been made to flow. However, it is felt that investigation of this possibility using the SEM would be very time-consuming. Any possible tendency toward rounding of the sharp edges of the Al_2O_3 particles is obscured by the large shape variations from particle to particle. The effects of the abrasion testing on the abrasives might be better characterized by using the same abrasive repeatedly in order to accentuate the shape and size changes so that they would be more readily distinguishable in the SEM.

2.4 Task IV- Wear Scar and Microstructure Characterization

Considerable previous effort has been expended in careful characterization of the microstructures of the alloys used in this study, and these results are briefly summarized here along with a description of more recent preliminary SEM characterizations of the wear scars.

2.4.1 Optical and Quantitative Metallography of the Co-base PM alloys

The metallographic characterization of the Co-base alloys has been discussed in detail in quarterly reports #5 and #6. Since the SEM/EDXS wear scar characterization completed to date and described in Section 2.4.3 of this report has centered on the Stellite 6 alloy, its microstructure is reproduced here in Figure 7. The microstructure consists of large Cr_7C_3 carbides in a Co-rich matrix. The volume fraction of these carbides is 33.8 percent. About 1.8 percent of the volume of the material is porosity.

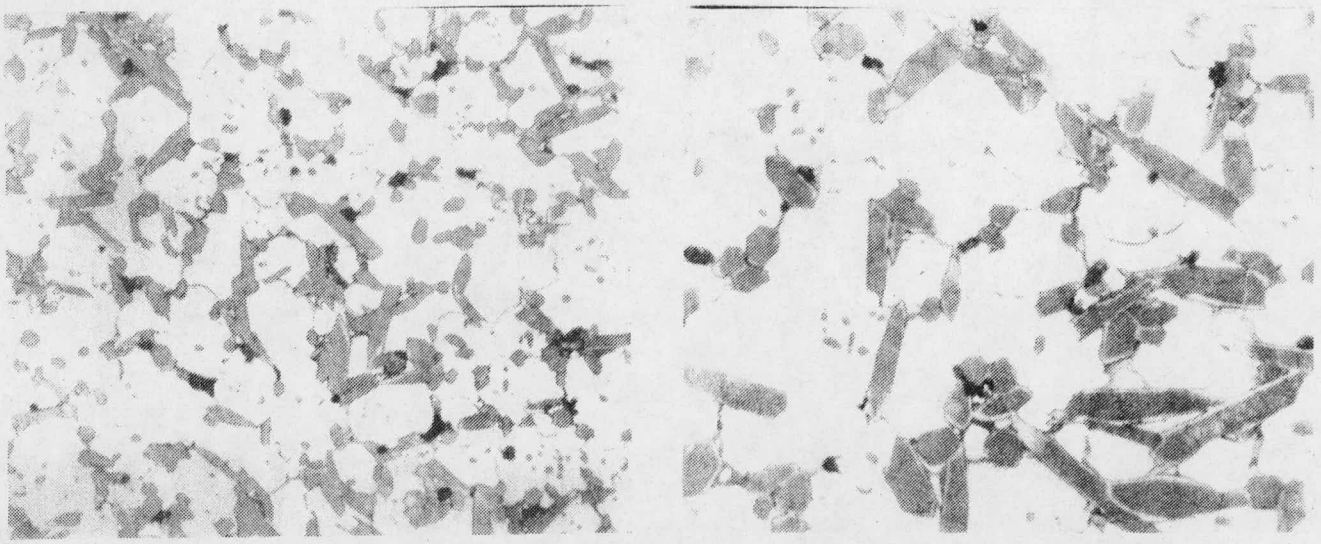

(a) (b)

Figure 7. Microstructure of Stellite 6, Cr_7C_3 carbides in Co-rich FCC matrix. (a) 320X , (b) 630X.

2.4.2 SEM Observations of Ni-Hard 4 Wear Scars.

SEM micrographs (secondary electron images) of the SiO_2 RWAT and the GAWT wear scars of the Ni-Hard 4 specimens were taken in an effort to correlate maxima and minima in wear rates (Figure 2) to changes in material removal mechanisms. The discussion of these observations is divided into two sections for convenience.

2.4.2.1 Ni-Hard 4 SiO_2 RWAT Wear Scars

Figures 8 through 11 show SEM micrographs of the SiO_2 RWAT wear scars for the Ni-Hard 4 specimens. Each figure shows at 500 and 1500X what often is termed the entrance region of the wear scar, where the abrasive first contacts the sample. Also shown are 500X micrographs of the central region of the scars. In each case, the entrance region of the wear scar contains raised areas which

(a)

(b)

(c)

Figure 8. SEM micrographs of SiO_2 RWAT wear scar of Ni-Hard 4 alloy with 5% γ. a) 500X, entrance region; b) 1500X, entrance region; c) 500X, central region.

(a)

(b)

(c)

Figure 9. SEM micrographs of SiO_2 RWAT wear scar of Ni-Hard 4 alloy with 20% γ. a) 500X, entrance region; b) 1500X, entrance region; c) 500X, central region.

(a)

(b)

(c)

Figure 10. SEM micrographs of SiO_2 RWAT wear scar of Ni-Hard 4 alloy with 40% γ. a) 500X, entrance region; b) 1500X, entrance region; c) 500X, central region.

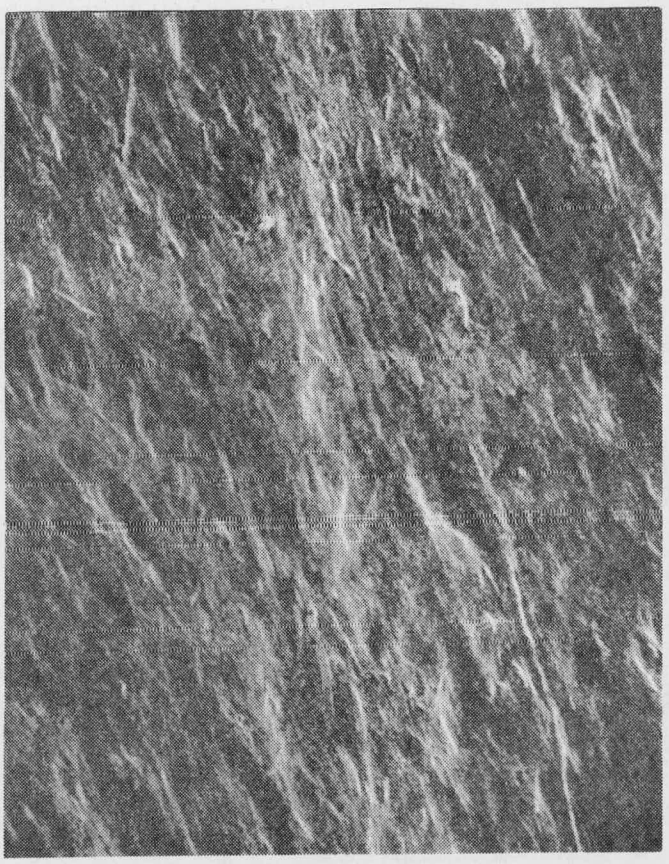

(a)

(b)

(c)

Figure 11. SEM micrographs of SiO_2 RWAT wear scar of Ni-Hard 4 alloy with 85% γ. a) 500X, entrance region; b) 1500X, entrance region; c) 500X, central region.

can be seen by comparison with the optical micrographs of Figure 1 to be of similar size and shape to the large carbides present in these alloys. Since the carbides are the hardest phase in the alloy it is concluded that they wear less rapidly than the matrices and therefore protrude from the surface in the entrance region. As will be seen, this conclusion is reinforced by the SEM/EDXS analysis of the Stellite 6 alloy, which indicates that carbides protrude from the RWAT wear scars.

The central region of the wear scar is much smoother and has less well-defined protrusions than the entrance region. It is of interest to note that the protrusions which do appear are most pronounced for the specimen with 40 percent retained austenite. Since this microstructure exhibited the highest RWAT wear rate, it might be supposed that a greater wear rate of the matrix was responsible. However, in view of the variations in contrast from one micrograph to the next, this is a tentative conclusion under further investigation.

Except for the evidence of a clear difference between the entrance and central regions of the wear scars, little information has been gained from the SEM investigation of the SiO_2 RWAT wear scars. It is not yet possible to conclusively identify the carbide locations relative to the raised areas in entrance or central regions of the wear scars because EDXS studies have not been conducted. Moreover, the smooth surface in the central region prevented more detailed examination of these areas at higher magnifications.

Although SEM examination of the worn surfaces is a good tool for finding qualitative differences in wear behavior (such as that between the entrance and central regions of the SiO_2 RWAT wear scars) it does not explain quantitatively differences in wear. It was not possible to determine from the SEM observations which alloy had experienced the highest wear rate, and this probably indicates that there is no significant change in wear mechanism either from sample to sample

or from position to position in a given sample.

2.4.2.2 Ni-Hard 4 GAWT Wear Scars

SEM micrographs of the GAWT wear scars are shown in Figures 12 through 15 for the four different microstructures of the Ni-Hard 4 alloy. These are qualitatively different from the SiO_2 RWAT scars as would be expected, since the test conditions are so different. In the GAWT test the hard abrasive particles are rigidly supported and cannot relax into the wheel as in the RWAT. Deep grooves are cut in the material surface, and since these grooves are long and continuous they must penetrate the carbides. The areas along the grooves where brittle fracture appears to have occurred are probably carbide locations, as can be seen by comparison with SEM/EDXS work on the Stellite 6 alloy. Attempts to correlate the features of the SEM micrographs to wear behavior were again unsuccessful. The specimen with 85 percent retained austenite appeared to have the deepest grooves, but contrast differences in the micrographs make comparisions difficult.

The SEM studies suggest that not all of the material displaced from a groove is removed from the surface of the target. There is certainly evidence that in some cases part of the material is extruded to the sides of the groove to form a thin ribbon of material which is still attached along one edge. These ribbons of material are often irregular and cracked and are probably easily removed from the surface by subsequent abrasive particles unless they are ploughed back into the surface. The fact that material which has been grossly plastically deformed remains attached to the worn surface may account for the shortcomings of abrasive wear theory. In the classical theory* an abrasive particle is assumed to plough a trough of material from the surface, and the material ploughed out is assumed to become free wear debris. The weight loss due to wear is calculated by summing the weight losses of the ploughed regions, i.e. the weight loss of the free debris. Since some of the displaced material remains attached to the target, the summation, and therefore the theory, is of limited accuracy.

*See for example E. Rabinowicz, Friction and Wear of Materials (Wiley, New York, 1965), p. 167.

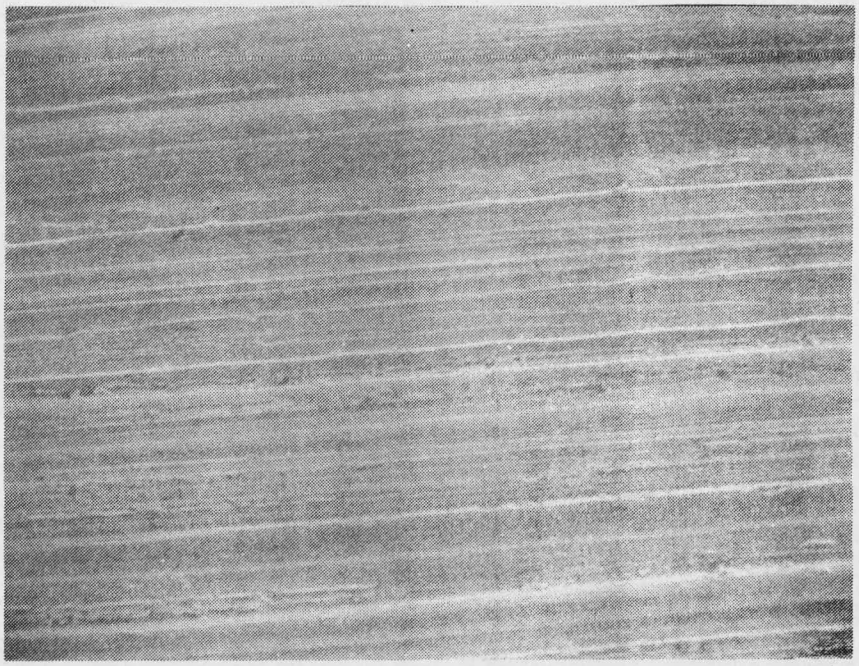

(a)

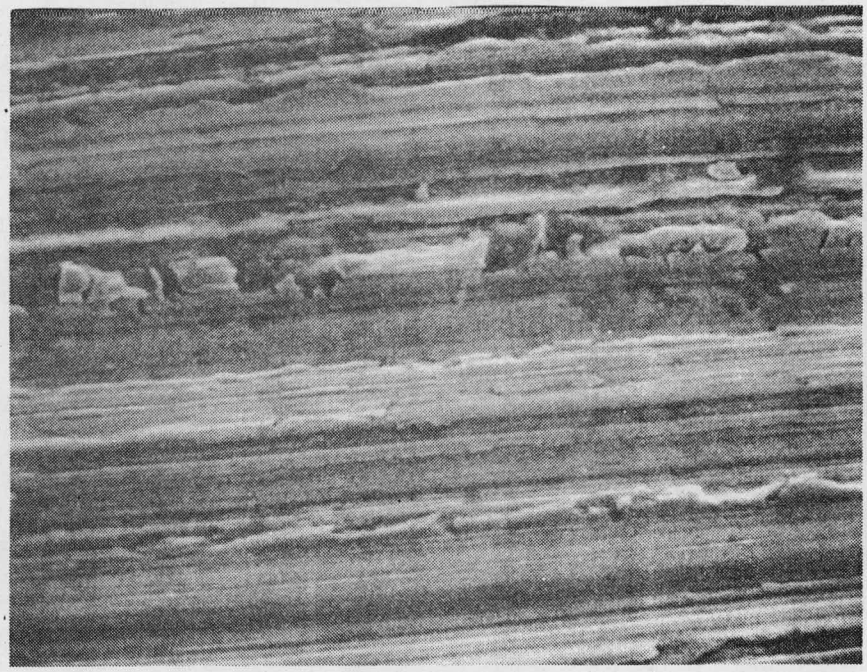

(b)

Figure 12. SEM micrographs of GAWT wear scar in Ni-Hard 4 alloy with 5% γ. (a) 200X; (b) 1000X.

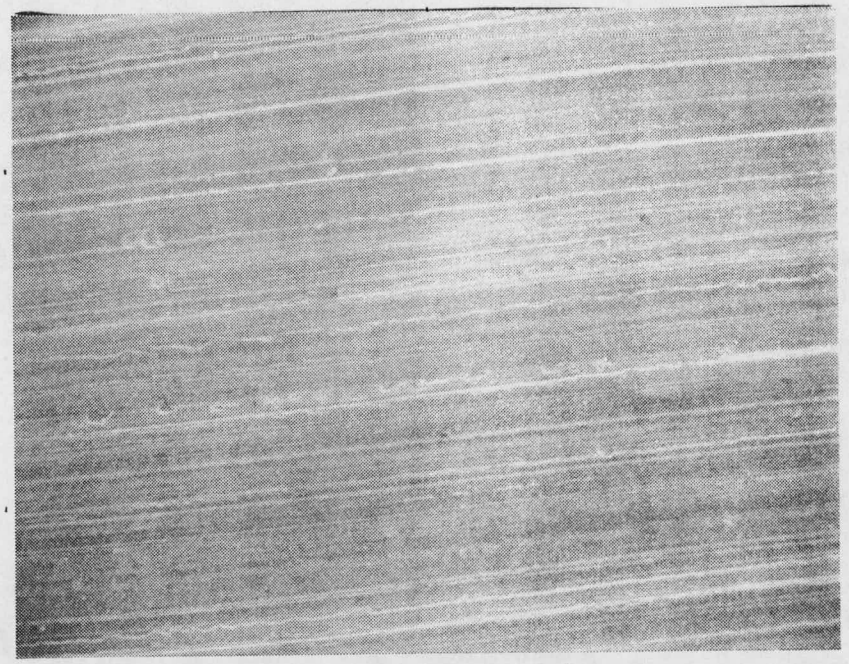

(a)

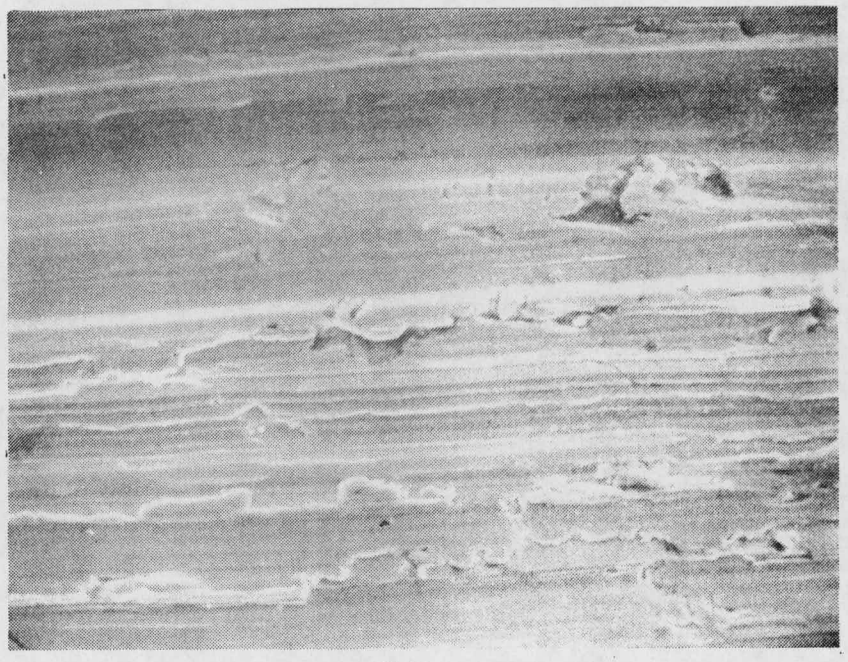

(b)

Figure 13. SEM micrographs of GAWT wear scar in Ni-Hard 4 alloy with 20% γ. (a) 200X; (b) 1000X.

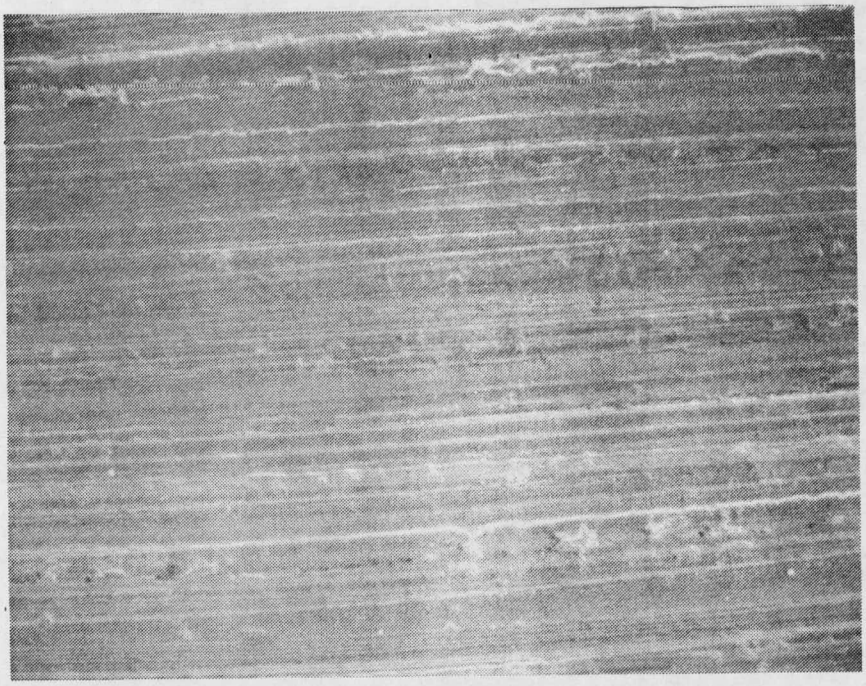

(a)

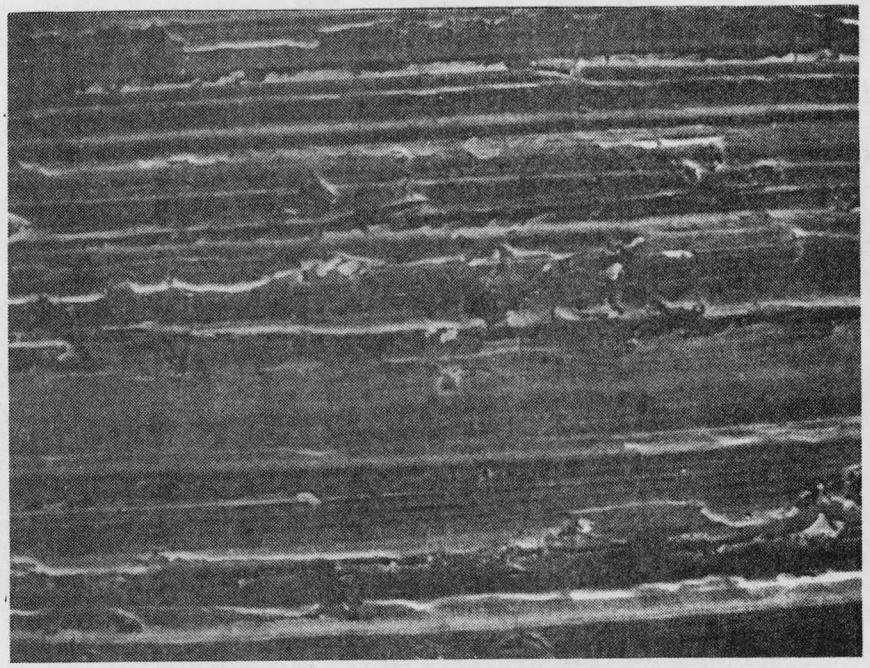

(b)

Figure 14. SEM micrographs of GAWT wear scar in Ni-Hard 4 alloy with 40% γ. (a) 200X; (b) 1000X.

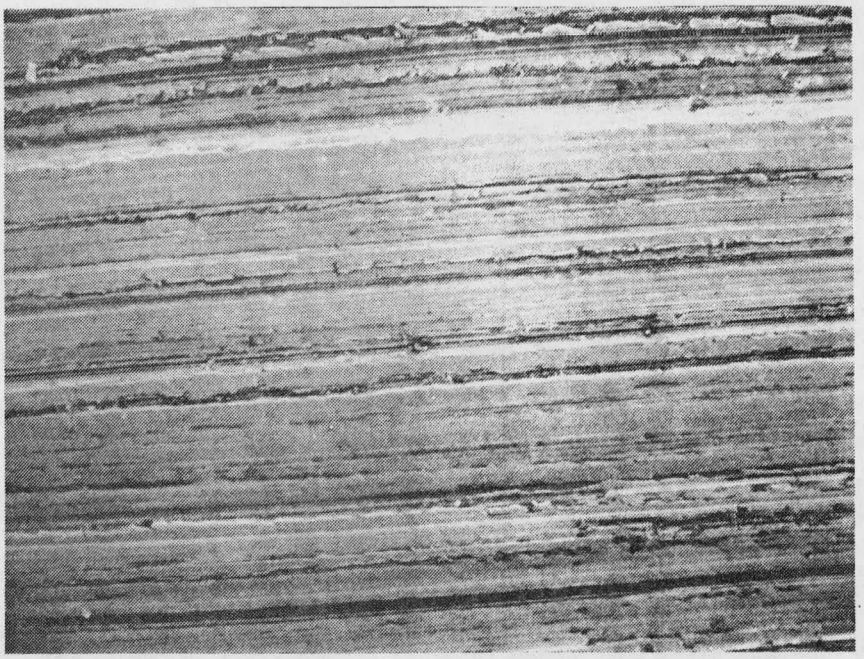

(a)

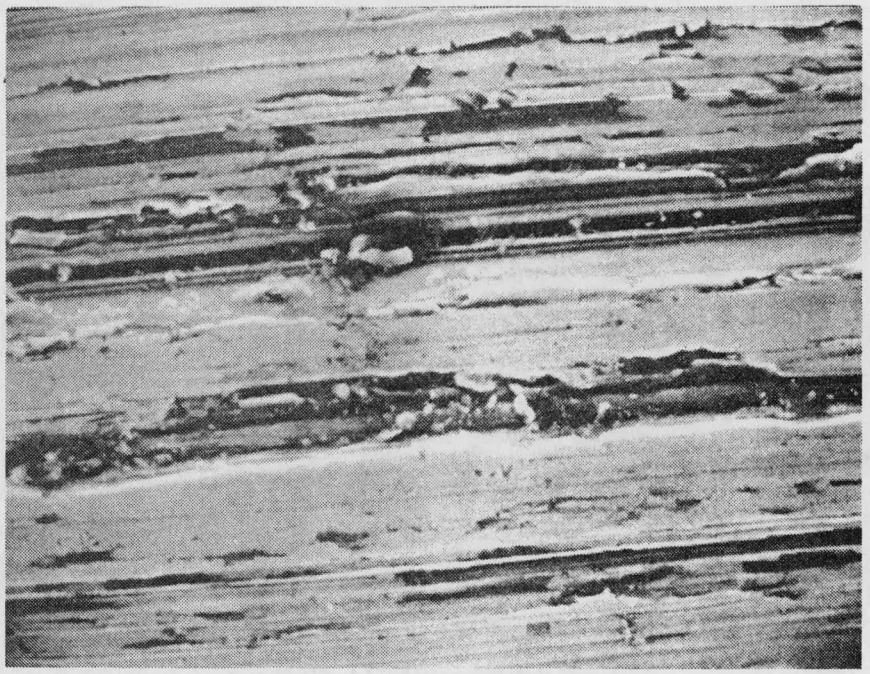

(b)

Figure 15. SEM micrographs of GAWT wear scar in Ni-Hard 4 alloy with 85% γ. (a) 200X; (b) 1000X.

2.4.3 SEM/EDXS Observations of Co-base PM Alloy Wear Scars

The SEM/EDXS analysis of the wear scars of the Co-base PM alloys has been begun by carefully studying the differences in the wear scars produced by the various tests on the same alloy. The Stellite 6 alloy was chosen for this purpose, and wear scars from both SiO_2 and Al_2O_3 RWAT tests and also from GAWT tests have been studied.

2.4.3.1 Co-base Alloy RWAT Wear Scars

Figures 16 through 19 show SEM secondary electron micrographs of the central regions of SiO_2 and Al_2O_3 RWAT wear scars of the Stellite 6 alloy. Each micrograph is accompanied by a chromium x-ray map, from the Princeton Gamma Tech (PGT) EDXS system. The maps reveal the carbides as areas of high Cr spot density.

These micrographs show clearly that in both the SiO_2 and the Al_2O_3 RWAT tests, carbides protrude from the central region of the wear scar. In the SiO_2 wear scars this tendency is more pronounced in the entrance region than in the central region, whereas in the Al_2O_3 RWAT wear scars the entrance and central regions are nearly indistinguishable.

The Al_2O_3 RWAT wear scars show deep grooves which are absent in specimens abraded with the softer, more rounded SiO_2 abrasive. These grooves also appear to penetrate the carbide particles,although the grooves generally become narrower as the abrasive particle passes over the carbide. It seems clear that the softer SiO_2 abrasive particles are forced to flow around and over the hard carbide particles without substantially damaging them. The carbides still provide some wear resistance against the hard Al_2O_3 abrasive, but they are not hard enough to prevent particle penetration in this case. These observations are in good agreement with the fact that the wear rate for the Al_2O_3 abrasive is about twenty times higher than that for the SiO_2 abrasive.

(a)

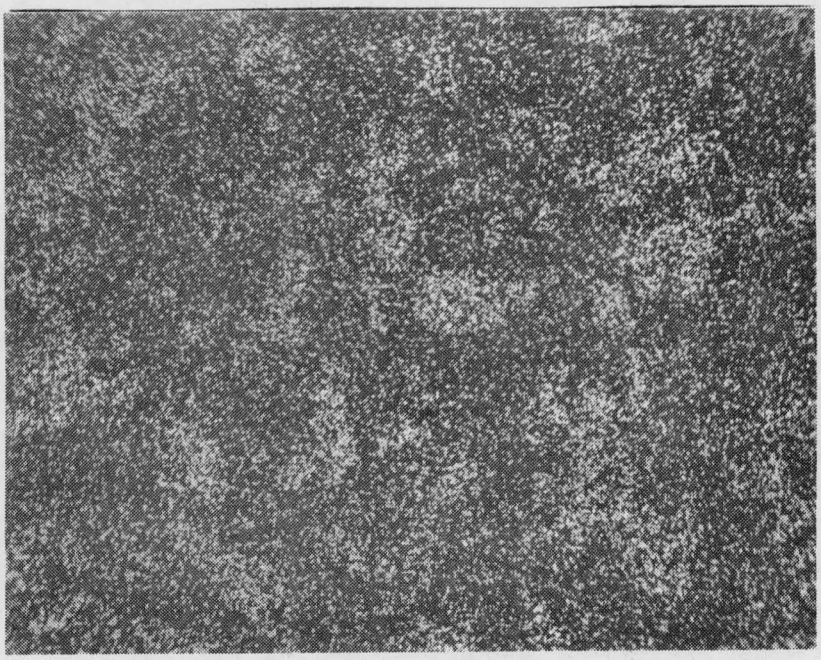

(b)

Figure 16. RWAT wear scar, new SiO_2, Stellite 6 alloy. (a) 700X; (b) Cr x-ray map; Cr_7C_3 carbides are located at areas of high spot density.

(a)

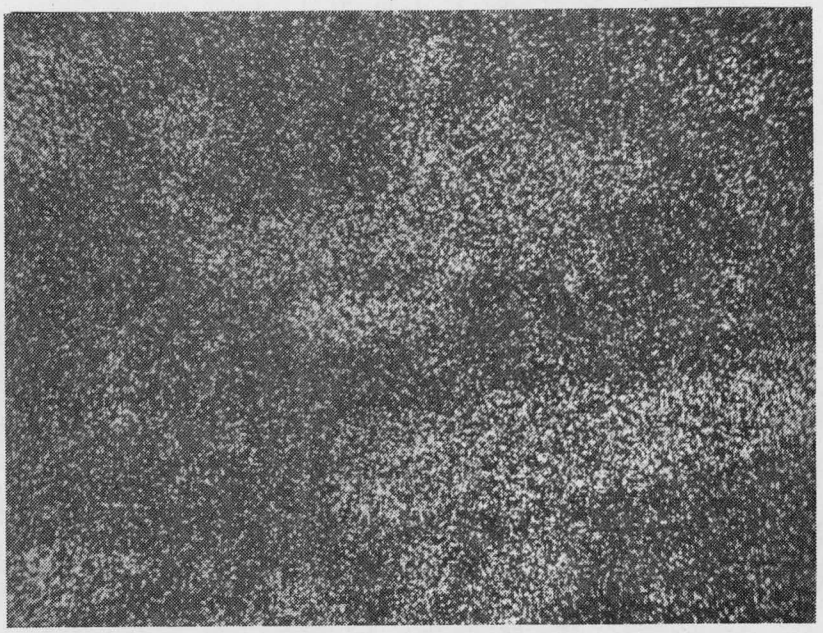

(b)

Figure 17. RWAT wear scar, new SiO_2, Stellite 6 alloy. (a) 2100X; (b) Cr x-ray map.

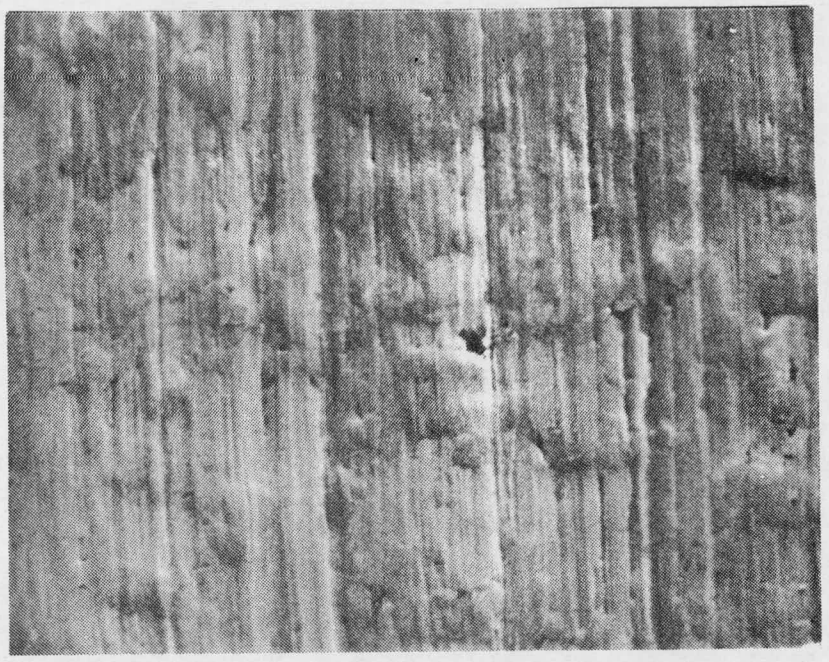

(a)

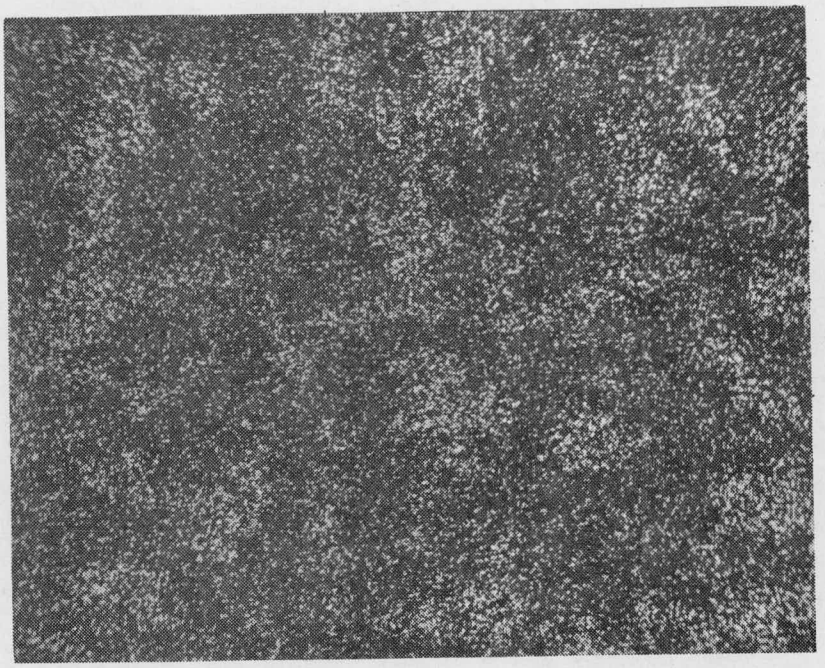

(b)

Figure 18. RWAT wear scar, new Al_2O_3, Stellite 6 alloy. (a) 700X; (b) Cr x-ray map.

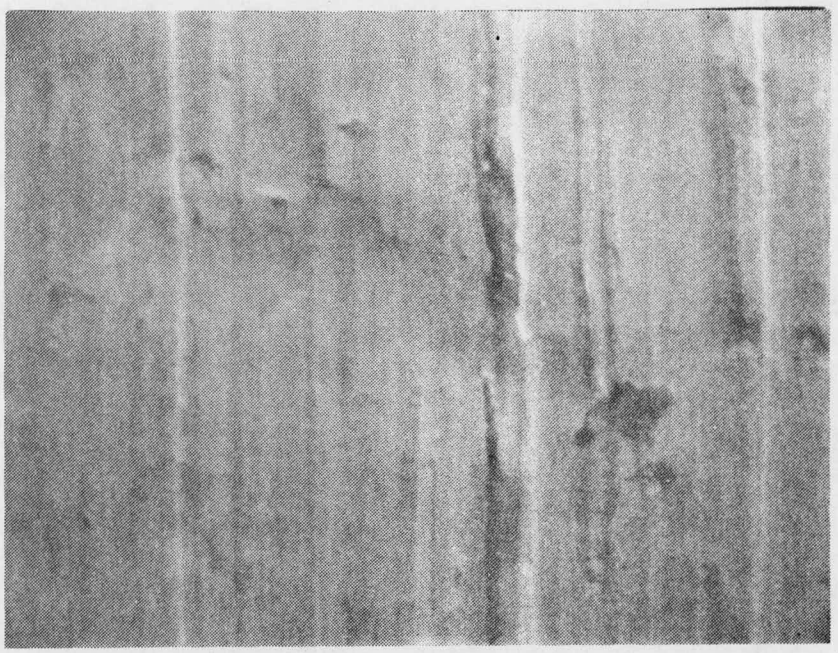

(a)

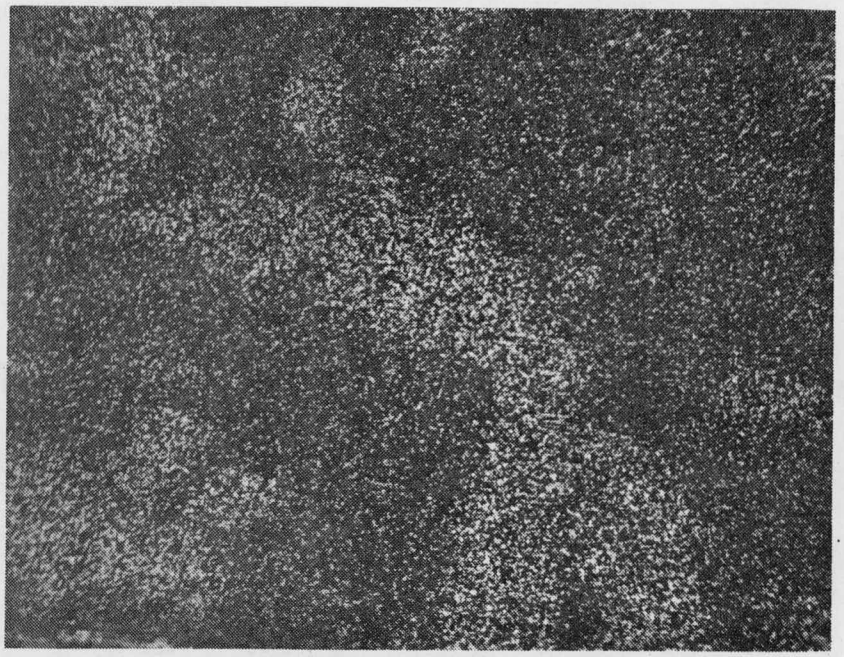

(b)

Figure 19. RWAT wear scar, new Al_2O_3, Stellite 6 alloy. (a) 2100X; (b) Cr x-ray map.

2.4.3.2 Co-base Alloy GAWT Wear Scars

Figures 20, 21 and 22 show SEM secondary electron micrographs and Cr x-ray maps of the GAWT wear scar for the Stellite 6 alloy. It is evident that the GAWT produces deep grooves in the material which penetrate the carbide particles. The carbide locations would not be apparent without the use of the EDXS Cr x-ray maps. These maps lead to the firm conclusion that the pits which are frequently observed in the worn surface are the sites of fractured carbide particles. Careful examination showed that all of the major pits in Figure 20 were carbide sites. In some cases, the broken carbides themselves appear to gouge material from the matrix as they are dragged out of the surface (Figure 22). Not all of the carbides are broken in this manner, however. Many are simply worn flush with the surface. The causes of the gross fracture of the carbides are not completely clear. They may fracture only after the major portion of the carbide has been removed, but the fracture process probably depends largely on the rake angle of the abrasive particle and the exact shape of the carbide. Since most of the carbides in any field of view have not undergone gross fracture, this fracture process may not contribute in a major way to material removal.

(a)

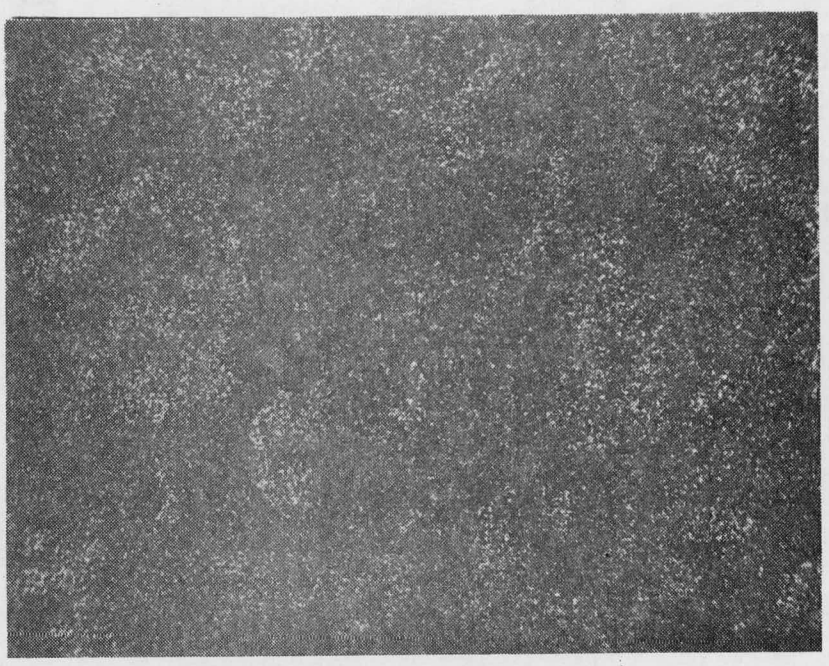

(b)

Figure 20. GAWT wear scar, Stellite 6 alloy. (a) 720X; (b) Cr x-ray map.

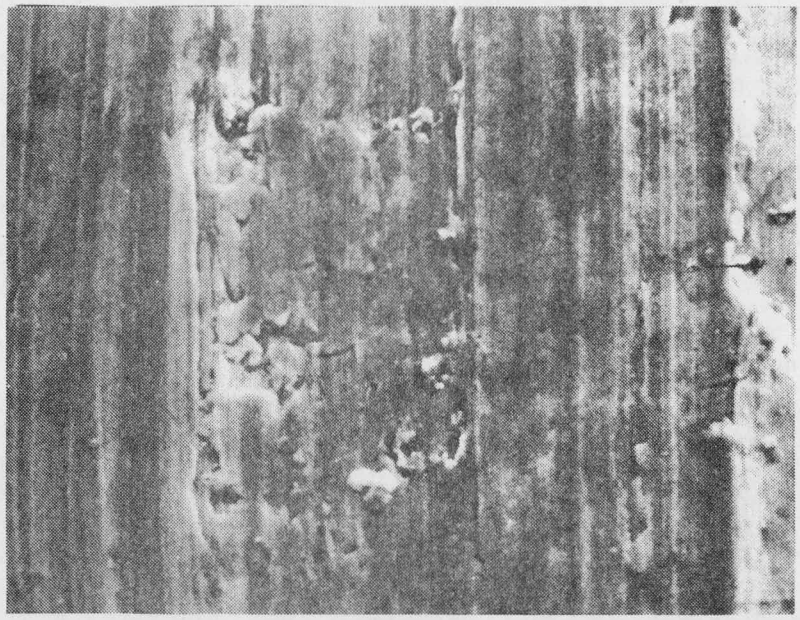

(a)

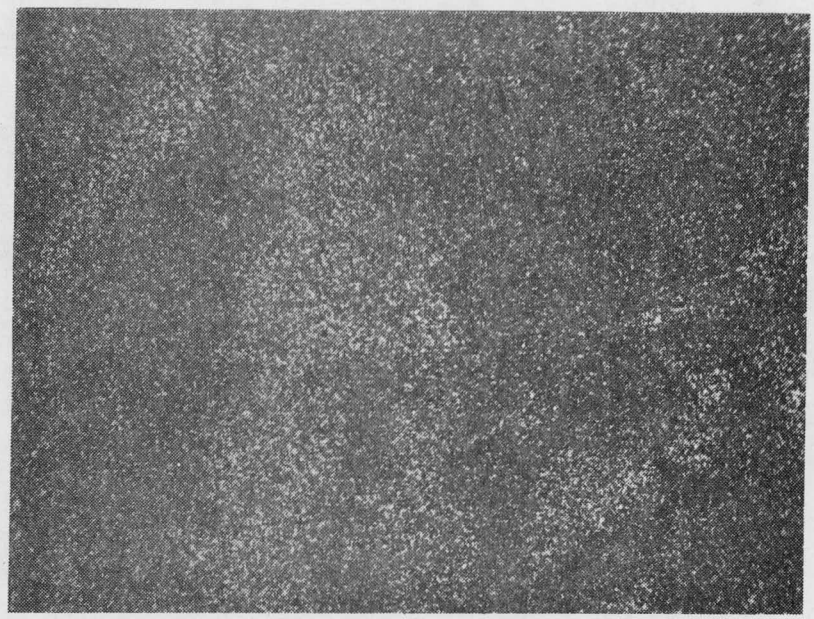

(b)

Figure 21. GAWT wear scar, Stellite 6 alloy. Same area as Figure 20. (a) 1800X; (b) Cr x-ray map.

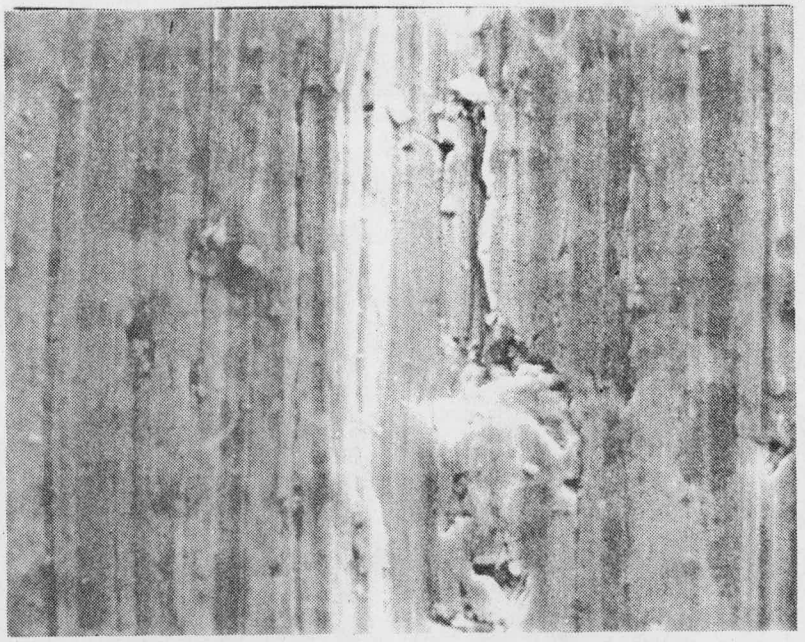

(a)

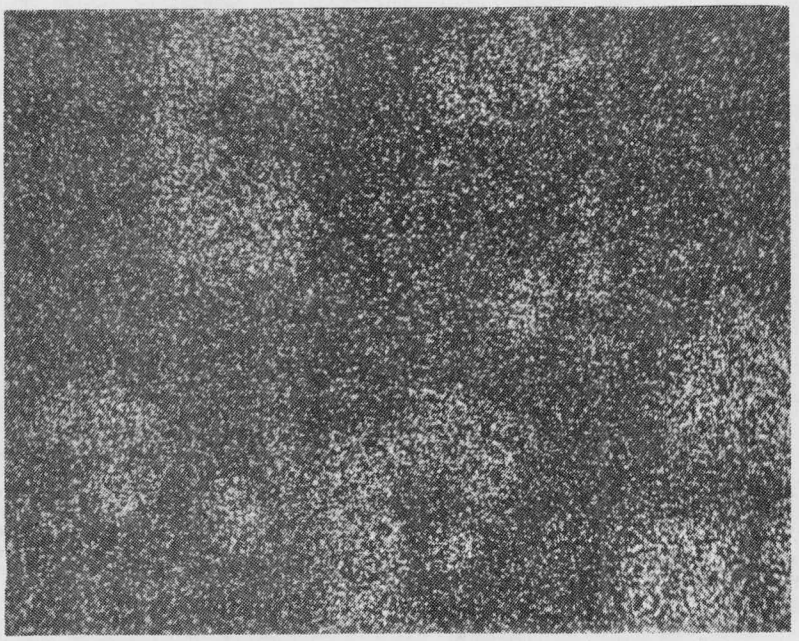

(b)

Figure 22. GAWT wear scar, Stellite 6 alloy, another area from Figure 20. (a) 1800X; (b) Cr x-ray map.

2.5 Task V - Analysis of Data

2.5.1 Ni-Hard 4 SEM Observations

As was discussed in section 2.4.2, the SEM observations of the RWAT and GAWT wear scars did not reveal any changes in the mechanisms of material removal for the Ni-Hard 4 samples. Furthermore, ranking of the wear resistance of the alloys by SEM observations was not possible. However, clear differences in the response of each material to the RWAT and GAWT tests were apparent. Although conclusive identification of the carbide locations relative to the raised areas in the RWAT wear scars was not possible at the time of these observations, the identification of protruding carbides in the Stellite 6 alloy RWAT wear scars strongly suggests that the raised areas in the Ni-Hard 4 RWAT wear scars are also protruding carbides.

Since the carbides appear in relief in the RWAT wear scars, they probably impart the major portion of the wear resistance of the alloys in this low-stress abrasion situation. However, the effects of carbide size, type and volume fraction must still be investigated. For example, the major carbide-attrition process in the RWAT is probably chipping away at edges. This supposition deserves more attention since it appears that the removal of material from the carbides may control the wear rate.

In the GAWT wear scars, the deep grooves observed indicate that the hard carbides are readily penetrated. Hence matrix strength may be of greater importance in gouging wear since the carbides and matrix are removed at equal rates.

It is instructive to note that the Ni-Hard GAWT wear scars appear to have much deeper surface grooves than the Stellite 6 GAWT wear scar. This suggests that groove depth might be a good indicator of wear rate, since the Ni-Hard 4 GAWT wear rates were all much higher than the Stellite 6 rates.

2.5.2 Co-base PM Alloy SEM Observations

The application of both EDXS techniques and SEM micrography yielded definite information concerning the role of the carbides in the Co-base PM alloys during RWAT and GAWT testing. As has been noted previously, in RWAT tests with both SiO_2 and Al_2O_3, abrasives, carbides protrude from the wear scars in the Stellite 6 alloy. It has also been found that long, continuous grooves are formed in the surface of this alloy in the Al_2O_3 RWAT test, and that these grooves cut across the carbides but are narrower in the carbides than in the matrix. These grooves are absent in the SiO_2 RWAT test, which produces a much lower wear rate. In the GAWT test, some of the carbides are cut off flush with the surface of the matrix, while some are broken apart and removed. The broken carbides sometimes gouge material from the matrix as they are dragged away. These observations are in sharp contrast to the observations of protruding carbides in the worn surface of the RWAT tests.

The degree to which the carbides are penetrated by the abrasive increases as the wear rate increases in the Stellite 6 alloy. That is, the abrasive particles do not appear to penetrate the carbides in the SiO_2 RWAT test, whereas they partially penetrate the carbides in the Al_2O_3 RWAT test and they completely penetrate the carbides in the GAWT test. While this is not a quantitative observation, it does show that the SEM observations are helpful in illustrating the differences in the response of an alloy to substantial changes in the severity of the abrasion conditions. It is hoped that further study will improve our ability to interpret the more subtle differences which are responsible for the differences in wear rates of the different alloys when they are subjected to the same testing conditions.

3. SUMMARY

In this quarter the major effort has been in the SEM study of the wear scars and of the abrasive particles.

The interpretation of the SEM micrographs of the new and used abrasive particles is hampered by the variety of shapes and textures present in the new abrasive. These variations mask any changes introduced by the abrasion test. Further investigation of the effect of the RWAT test on the abrasive could be done either by careful observations of individual particles before and after use in the RWAT test or by observation of abrasive which had been used repeatedly to accentuate the effects of the degradation.

The preliminary study of the Ni-Hard 4 wear scars was done without the advantage of the use of EDXS techniques to determine the carbide locations in the worn surface. However, the later observations of the Co-base PM alloy wear scars have been of value in confirming the interpretation of the SEM observations on the Ni-Hard 4 wear scars.

The SEM/EDXS study of the wear scars of the Co-base PM alloys has been begun by investigating the wear scars of the Stellite 6 alloy from three different abrasion conditions. (RWAT new SiO_2, new Al_2O_3, GAWT). This was done in order to determine what effects large changes in abrasion test conditions would produce on wear rates and the worn surface. It has been shown that definite changes in the response of the carbides can be demonstrated when the test conditions are changed. The next phase of the wear scar characterization will involve observations of the wear scars of the other Co-base PM alloys. The information gained will be used to analyze the microstructural features which are responsible for the wear resistance trends found in these alloys.

4. PERSONNEL

The co-principal investigators, Dr. N. F. Fiore and Dr. T. H. Kosel have devoted 20% and 10% effort respectively to the project during this quarter. Two graduate research assistants, Mr. W. Konkel and Mr. S. Udvardy, have devoted 50% effort.

LIST OF FIGURES

Figure 1. Microstructures resulting from the four different heat treatments of the Ni-Hard 4 cast iron. M_7C_3 carbides (white) in matrices of various percentages of retained austenite with austenite decomposition products. (a) 5% γ; (b) 20% γ; (c) 40% γ; (d) 85% γ. All are at 900X. 3

Figure 2. RWAT, APT, and GAWT test results on Ni-Hard 4 samples. The percent retained austenite decreases toward the right. 4

Figure 3. GAWT abrasion factor and RWAT weight loss (unused and used SiO_2) versus carbide volume fraction. 5

Figure 4. RWAT weight loss (unused and used Al_2O_3) versus carbide volume fraction. 5

Figure 5. Sieve analyses of new and used RWAT abrasives. (a) SiO_2 and (b) Al_2O_3. 6

Figure 6. 60X SEM micrographs of new and used RWAT abrasives. (a) New SiO_2, (b) SiO_2, used twice, (c) new Al_2O_3, and (d) Al_2O_3, used twice. 7

Figure 7. Microstructure of Stellite 6, Cr_7C_3 carbides in Co-rich FCC matrix. (a) 320X, (b) 630X. 9

Figure 8. SEM micrographs of SiO_2 RWAT wear scar of Ni-Hard 4 alloy with 5% γ. (a) 500X, entrance region; (b) 1500X, entrance region; (c) 500X, central region. 10

Figure 9. SEM micrographs of SiO_2 RWAT wear scar of Ni-Hard 4 alloy with 20% γ. (a) 500X, entrance region; (b) 1500X, entrance region; (c) 500X, central region. 11

Figure 10. SEM micrographs of SiO_2 RWAT wear scar of Ni-Hard 4 alloy with 40% γ. (a) 500X, entrance region; (b) 1500X, entrance region; (c) 500X, central region. 12

Figure 11. SEM micrographs of SiO_2 RWAT wear scar of Ni-Hard 4 alloy with 85% γ. (a) 500X, entrance region; (b) 1500X, entrance region; (c) 500X, central region. 13

Figure 12. SEM micrographs of GAWT wear scar in Ni-Hard 4 alloy with 5% γ. (a) 200X; (b) 1000X. 16

Figure 13. SEM micrographs of GAWT wear scar in Ni-Hard 4 alloy with 20% γ. (a) 200X; (b) 1000X. 17

Figure 14. SEM micrographs of GAWT wear scar in Ni-Hard 4 alloy with 40% γ. (a) 200X; (b) 1000X. 18

LIST OF FIGURES (continued)

Figure 15. SEM micrographs of GAWT wear scar in Ni-Hard 4 alloy with 85% γ. (a) 200X; (b) 1000X. 19

Figure 16. RWAT wear scar, new SiO_2, Stellite 6 alloy. (a) 700X; (b) Cr x-ray map; Cr_7C_3 carbides are located at areas of high spot density. 21

Figure 17. RWAT wear scar, new SiO_2, Stellite 6 alloy. (a) 2100X; (b) Cr x-ray map. 22

Figure 18. RWAT wear scar, new Al_2O_3, Stellite 6 alloy. (a) 700X; (b) Cr x-ray map. 23

Figure 19. RWAT wear scar, new Al_2O_3, Stellite 6 alloy. (a) 2100X; (b) Cr x-ray map. 24

Figure 20. GAWT wear scar, Stellite 6 alloy. (a) 720X; (b) Cr x-ray map. 26

Figure 21. GAWT wear scar, Stellite 6 alloy. Same area as Figure 20. (a) 1800X; (b) Cr x-ray map. 27

Figure 22. GAWT wear scar, Stellite 6 alloy. Another area from Figure 20. (a) 1800X; (b) Cr x-ray map. 28

DISTRIBUTION LIST

Mr. John J. Mahoney
Senior Contract Administrator
Contracts Management Office
DOE- Chicago Operations Office
9700 South Cass Avenue
Argonne, IL 60439
- 6 copies -

Dr. S. J. Dapkunas
Division of System Engineering/
Energy Technology
U.S. D.O.E.
Room C-155
Germantown, MD 21401
- 3 copies -

Dr. Paul Scott
Division of System Engineering/
Energy Technology
U.S. D.O.E.
Room C-155
Germantown, MD 21401

Dr. Sam Schneider
National Bureau of Standards
Washington, D.C. 20234

Dr. John Dodd
Climax Molybdenum Company
13949 West Colfax Avenue
Golden, CO 80401

Metals and Ceramics Information Center
Battelle-Columbus Laboratories
505 King Avenue
Columbus, OH 43201

Dr. J. L.Parks
Climax Molybdenum Research Lab
1600 Huron Parkway
Ann Arbor, MI 48106

Dr. M. S. Bhat
Materials and Molecular Research Div.
Bldg. 62 - Room 239
Lawrence Berkeley Laboratory
University of California
Berkeley, CA 94720

Mr. Howard Avery
69 Alcott
Mahwah, N.J. 07430

Dr. Kenneth Antony
Stellite Division
Cabot Corporation
Kokomo, IN 46901

Dr. Stanley Wolf
Materials Science Program
Basic Energy Sciences Division
D.O.E.
Washington, D.C. 20545

Dr. Joseph Klein
Stellite Division
Cabot Corporation
Kokomo, IN 46901

Dr. Jerry L. Arnold
Research and Technology
Armco Steel Corporation
Middletown, OH 45043

Dr. R. C. Tucker
Union Carbide Corp.
1500 Polco Street
Indianapolis, IN 46224

Dr. Paul Swanson
Deere and Company Technical Center
3300 River Drive
Moline, IL 61265

Dr. Jeffrey S. Hansen
P.O. Box 70
Bureau of Mines
Albany, OR 97321

Dr. R. J. Dawson
Falconbridge Nickel Mines Ltd.
P.O. Box 900, 8810 Yonge St.
Thornhill, Ontario, Canada L3T 4A8

Dr. Burton R. Patterson
Southern Research Institute
2000 Ninth Avenue, South
Birmingham, AL 35205